Improved understanding of soil moisture variability dynamics

Adriaan J. Teuling and Peter A. Troch

Hydrology and Quantitative Water Management Group, Wageningen University, Wageningen, Netherlands

[1] Different trends of soil moisture variability with mean moisture content have been reported from field observations. Here we explain these trends for three different data sets by showing how vegetation, soil and topography controls interact to either create or destroy spatial variance. Improved understanding of these processes is needed for the transformation of point-scale measurements and parameterizations to scales required for climate studies, operational weather forecasting, and large scale hydrological modeling. **Citation:** Teuling, A. J., and P. A. Troch (2005), Improved understanding of soil moisture variability dynamics, *Geophys. Res. Lett.*, *32*, L05404, doi:10.1029/2004GL021935.

1. Introduction

[2] Although the quantitative contribution of soil moisture to the global water budget is negligible, it plays a central role in the global water cycle by controlling the partitioning of water and energy fluxes at the earth's surface, and may control the continental water distribution through land-surface atmosphere feedback mechanisms [*Koster et al.*, 2003]. The ability of coupled models to reproduce these processes will strongly depend on the parameterization of soil moisture state-flux relationships at the regional scale. The lack of accurate observations of land surface states and fluxes at this scale, combined with the variability of soil moisture and the high non-linearity of land-surface processes at the small scale, requires aggregation of small scale processes to larger scales in order to prevent systematic biases in modeled water- and energy fluxes [*Crow and Wood*, 2002]. For successful aggregation, knowledge on soil moisture variability controls is indispensable.

[3] Several scientists have reported soil moisture variability to increase with decreasing mean moisture content [e.g., *Famiglietti et al.*, 1999; *Hupet and Vanclooster*, 2002]. Other scientists reported opposite trends [e.g., *Western and Grayson*, 1998; *Famiglietti et al.*, 1998], were unable to detect a trend [e.g., *Hawley et al.*, 1983; *Charpentier and Groffman*, 1992], or found the trend to depend on the mean soil moisture state [e.g., *Owe et al.*, 1982; *Albertson and Montaldo*, 2003]. Although many scientists have speculated about the origin of soil moisture variability, there have been only few quantitative studies looking at how different processes act to either increase or decrease the spatial variability of soil moisture. By using the similar media concept, *Salvucci* [1998] showed how variability in soil texture leads to different soil moisture variability states in different limiting cases. *Albertson and Montaldo* [2003] showed how covariances between soil

moisture and fluxes, originating from variability in soil moisture, forcing and/or land surface properties, can lead to either an increase or decrease in soil moisture variability.

[4] Here we develop a simple model that is able to reproduce the different observed soil moisture variability trends for the three different data sets that were used in this study (see Figures 1 and top panels of Figure 2). We also show that the apparent contradictory observations can be explained by the temporal dynamics of the interaction between soil, vegetation, and topography controls.

2. Data

[5] Soil moisture (0–20 cm) variability was measured at an agricultural field in Louvain-la-Neuve (Belgium) on 60 days between 30 May 1999 and 13 September 1999 as part of a campaign with the objective to investigate the within-field spatial variability of transpiration [*Hupet and Vanclooster*, 2002]. The soils in the field are classified as well-drained silty-loam and there is little relief. During the campaign the field was cropped with maize. The climate is moderate humid. Meteorological observations are available from 1 January 1999 till 31 December 1999.

[6] From 24 June 1998 to 26 January 1999, soil moisture (0–30 cm) was measured with 36 TDR sensors (spacing 1 m) at a gently sloping field transect at the Virginia Coastal Reserve Long Term Ecological Research (VCR-LTER) site on the eastern shore of Virginia [*Albertson and Montaldo*, 2003]. The sandy loam soils were covered by Johnson grass. Meteorological observations are available for the period 30 June 1998 till 27 September 1998.

[7] The Australian Tarrawarra dataset results from an experiment that aimed at investigating the spatial pattern of soil moisture at the small catchment scale. Between 27 September 1995 and 29 November 1996 a total of 13 soil moisture (0–30 cm) patterns were measured [*Western and Grayson*, 1998]. Additional measurements are summarized by *Western et al.* [2004]. The soils in the catchment are silty-loam to clay, and the topography is undulating with a maximum relief of 27 m. The climate is temperate. Land use is perennial pastures used for grazing. Meteorological observations are available for the period 10 August 1995 till 25 October 1997.

3. Modeling Variability
3.1. Point-Scale Soil Moisture Dynamics

[8] Under most conditions, lateral flow in the upper part of the soil can be neglected, and the vertically integrated soil moisture balance over a depth L can be written as:

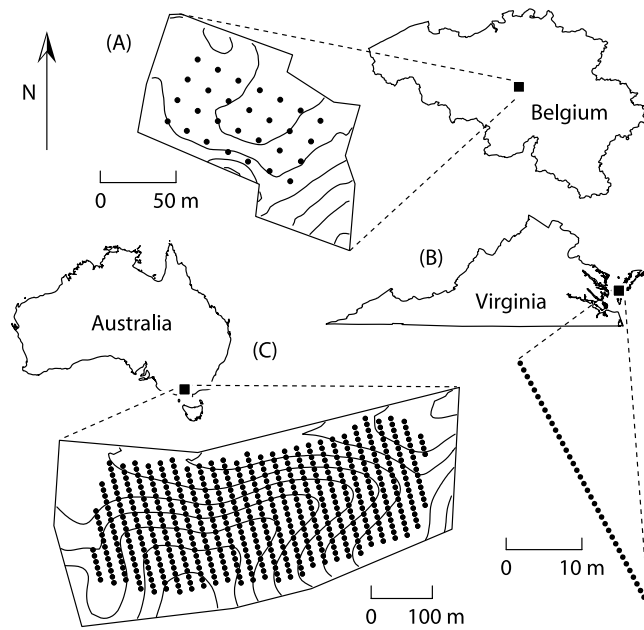$$\frac{d\theta}{dt} = \frac{1}{L}(T - R - q - S) \tag{1}$$

Figure 1. Location of observation sites: (a) Louvain-la-Neuve, with 0.5 m contour lines, (b) VCR-LTER site, (c) Tarrawarra, with 2 m contour lines.

where θ is the volumetric soil moisture content averaged over a depth L, T the throughfall, R the saturation excess runoff, q the deep drainage, and S the root water uptake. Here $L = 0.5$ m. Throughfall is the rainfall P that is not intercepted by vegetation. The size of the interception reservoir is taken proportional to the leaf area index ξ, with a proportionality constant of 0.2 mm, and the reservoir is assumed to evaporate every day. Since $0 \leq \theta \leq \phi$, where ϕ is the porosity, R equals T for $\theta = \phi$ and is 0 for $\theta < \phi$. We assume bare soil evaporation to be small in comparison to the root uptake over the entire profile. Drainage is calculated using Darcy's law with the unit-gradient assumption. Using the *Campbell* [1974] parameterization yields:

$$ q = k_s \left(\frac{\theta}{\phi} \right)^{2b+3} \qquad (2) $$

where k_s is the saturated hydraulic conductivity, and b a pore size distribution parameter. We write the vertically integrated root water uptake S as:

$$ S = f_r \beta [1 - \exp(-c\xi)] E_p \qquad (3) $$

where f_r is the root fraction in the layer of depth L, β a soil moisture stress function, c a light use efficiency parameter, and E_p the potential evapotranspiration. The factor $1 - \exp(-c\xi)$ allows for spatially variable response of unstressed transpiration to atmospheric boundary layer conditions [*Al-Kaisi et al.*, 1989]. For Louvain-la-Neuve, the positive relation between ξ and S was confirmed by *Hupet and Vanclooster* [2004]. Soil moisture stress is modeled as:

$$ \beta = \max \left[0; \min \left(1; \frac{\theta - \theta_w}{\theta_c - \theta_w} \right) \right] \qquad (4) $$

where the critical moisture content θ_c defines the transition between unstressed and stressed transpiration, and the wilting point θ_w the point below which plants are no longer able to extract water from the soil matrix. Land cover (or ξ) is modeled with a spatial and temporal component:

$$ \xi = \xi_{max} \left[c_1 - (1 - c_1) \sin \left(2\pi \frac{DOY - c_2}{c_3} + \frac{\pi}{2} \right) \right] \qquad (5) $$

where ξ_{max} is the local maximum of ξ, and c_i specify the seasonal development of ξ. The model defined by (1)–(5) sufficiently captures the non-linearities and dynamics of the soil moisture loss processes, and similar models have proven successful in reproducing point scale soil moisture dynamics [e.g., *Albertson and Kiely*, 2001; *Laio et al.*, 2001]. Here we choose a simple model since adding more complexity to the model as presented would result in an increasing number of (generally unknown) covariances between the parameters. In order to match the observed forcing, the model was integrated to yield daily values.

3.2. Spatial Closure

[9] We reproduce the first and second order spatial moments of θ ($\bar{\theta}$ and σ_m^2) by running a large ensemble of the model defined by (1)–(5) with variable parameters. Initial conditions of θ are set by adjusting θ to a spatially uniform q of 1 mm d^{-1}. We assume both $\ln(k_s)$ and ξ_{max} to follow a normal distribution with parameters $\mu_{k,\xi}$ and $\sigma_{k,\xi}$. Since ϕ and b are generally correlated with k_s, we related these to k_s by linear regression with $\ln(k_s)$, fitted to the data provided by *Clapp and Hornberger* [1978]. This yields $\phi = -0.0147\ln(k_s) + 0.545$ and $b = -1.24\ln(k_s) + 15.3$. Due to the positive effect of high k_s on canopy growth through better aeration, soil temperature and water transport to roots, we assume a (perfect) positive linear correlation between $\ln(k_s)$ and ξ_{max}. Other vegetation parameters are taken as constants. Atmospheric forcing (P and E_p) was calculated from available observations and assumed to be constant in space.

3.3. Total Simulated Variability

[10] In order to account for spatial differences in the water balance caused by differences in exposure due to sloping of the landscape, we follow *Svetlitchnyi et al.*
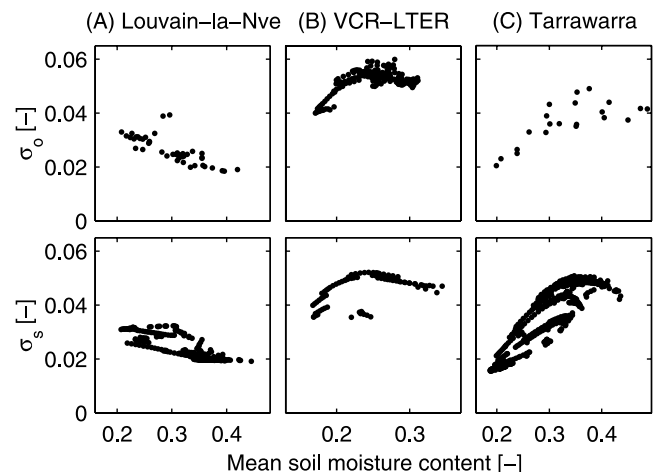

Figure 2. Observed (σ_o) and simulated (σ_s) soil moisture variability versus mean soil moisture content ($\bar{\theta}$).

Table 1. Parameter Values Used in the Simulation of σ_s

Parameter	Louvain-la-Nev	VCR-LTER	Tarrawarra
μ_k, σ_k ln[mm d^{-1}]	5.6, 0.63[a]	6.5, 1.0	5.2, 0.96[a]
θ_w [-]	0.15ϕ	0.22ϕ[b]	0.35ϕ
θ_c [-]	0.44ϕ	0.50ϕ[b]	0.67ϕ
μ_ξ, σ_ξ [-]	3.6, 0.50[a]	3.6, 0.50	6.0, 1.0[c]
c [-]	0.55[d]	0.40	0.40
f_r [-]	0.90	0.80	1
c_1, c_2, c_3 [-,d,d]	0.5,114,260[e]	1,-,-	0.5,139,365[c]
σ_η [-]	N/A	N/A	0.1530[f]
ϵ [-]	0.005	0.005	0.013[g]

[a]Fitted from observations.
[b]Adapted from *Albertson and Kiely* [2001].
[c]Estimated from biomass measurements assuming a specific leaf area of 0.02 m^2 g^{-1}.
[d]From *Al-Kaisi et al.* [1989].
[e]For $114 \leq$ DOY ≤ 283, else 0.
[f]Derived from a 5 × 5 m digital elevation model.
[g]From *Western and Grayson* [1998].

[2003] and write the non-local effect of topography (subscript t) on the distribution of available soil moisture $\theta^* = \theta - \theta_w$ in the top 0.5 m of the soil in terms of a wetness coefficient η and the expected value of θ^* for a flat surface:

$$\theta_t^* = \eta \overline{\theta^*} \qquad (6)$$

[11] In (6), local values of η depend on slope profile shape, slope aspect, distance from the divide, and slope gradient [*Svetlitchnyi et al.*, 2003], and can be derived from a digital elevation model. As a first order approach, we add the variance caused by (6) to σ_m^2, assuming $\overline{\eta} = 1$. To allow direct comparison with observations, we also account for apparent variability due to a (bias-free and stationary) measurement error ϵ. The total simulated soil moisture variance σ_s^2 can now be written as:

$$\sigma_s^2(t) = \sigma_m^2(t) + \sigma_\eta^2 \overline{\theta^*}^2(t) + \epsilon^2 \qquad (7)$$

[12] The parameters used in the simulations of σ_s are summarized in Table 1.

4. Analysis

[13] Figure 2 shows that both the range of $\overline{\theta}$ as well as the magnitude, trend, and hysteresis effects of σ_s for the different data sets compare well to the observations. In order to distinguish the contribution of different controls on the time evolution of σ_s, we derive an expression for $d\sigma_s^2/dt$ as a function of these controls. Subtracting the spatial average equivalent of (1) from (1) yields an expression for the time evolution of a local soil moisture anomaly:

$$\frac{d\theta'}{dt} = \frac{1}{L}(T' - R' - q' - S') \qquad (8)$$

where $'$ denotes a deviation from the spatial average. Multiplying (8) by $2\theta'$, performing a chain rule operation to the left hand side, and averaging the result yields:

$$\frac{d\overline{\theta'^2}}{dt} = \frac{d\sigma_m^2}{dt} = \frac{2}{L}\left(\overline{\theta'T'} - \overline{\theta'R'} - \overline{\theta'q'} - \overline{\theta'S'}\right) \qquad (9)$$

which is the expression for the time evolution of the spatial soil moisture variance derived by *Albertson and Montaldo* [2003] but applied to our balance equation (1). Since the right-hand side of (9) consists of covariance terms, their contribution depends on both the magnitude of soil moisture and flux anomalies as well as their mutual correlation. The sign of the correlation controls whether the different processes act to create or destroy spatial soil moisture variance (for synthetic examples, see *Albertson and Montaldo* [2003]). Combining (9) with the time derivative of (7) yields:

$$\frac{d\sigma_s^2}{dt} = \underbrace{\frac{2}{L}\left(\overline{\theta'T'} - \overline{\theta'S'}\right)}_{\text{Vegetation}} - \underbrace{\frac{2}{L}\left(\overline{\theta'R'} + \overline{\theta'q'}\right)}_{\text{Soil}} + \underbrace{\sigma_\eta^2 \frac{d\overline{\theta}^2}{dt}}_{\text{Landscape}} \qquad (10)$$

[14] In stead of evaluating all terms separately, we group the correlated terms as (local) vegetation and soil controls, and non-local landscape control. Figure 3 explains the different trends in Figure 2 by evaluating the contribution of the different groups in (10). For clarity the terms have been converted to monthly averages. Note that inherently to our stochastic approach, the numbers in Figure 3 should be considered as indicative rather than exact. Since drainage is generally a fast process compared to evapotranspiration [*Albertson and Kiely*, 2001], much of the soil contributions in Figure 3 take place within days following major precipitation events. Daily values of the vegetation contribution are of lower magnitude, but show less spread.

[15] In the Louvain-la-Neuve dataset, soil moisture variability increases during the growing season. During winter and spring (December–April), precipitation surplus causes
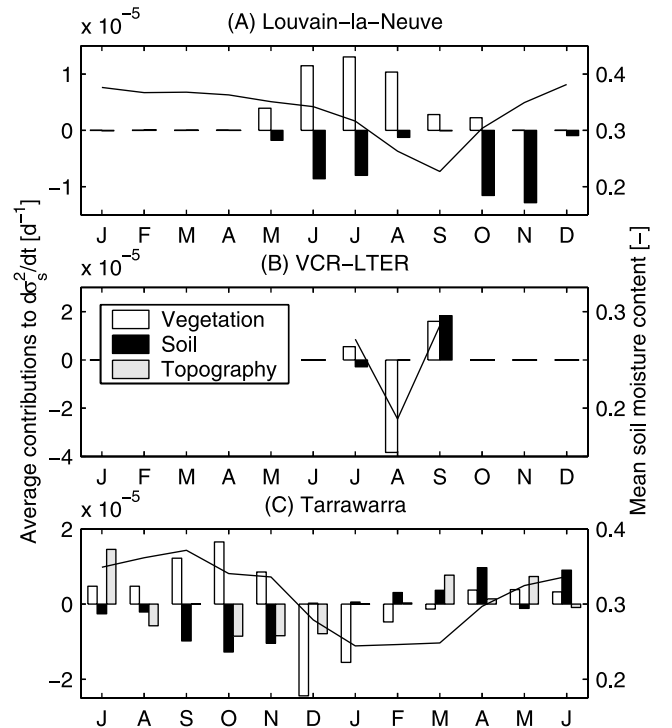

Figure 3. Monthly average vegetation, soil, and landscape contributions to $d\sigma_s^2/dt$, as in (10), and mean soil moisture content ($\overline{\theta}$).

soil moisture to remain near field capacity, and the variance is fully adjusted to the soil footprint (Figure 3a). Here the soil footprint is the soil moisture variance under constant q. Until July, increases in variance due to heterogeneous transpiration are effectively (although not entirely) cancelled out by drainage. When drainage becomes negligible (August–September), spatially variable water uptake by vegetation acts to create additional variance. This increase is only destroyed during the first rainfall events in the late growing season (October–November), when the variance is "reset" to that of the soil footprint ($\overline{\theta' q'} > 0$). It should be noted that even during summer root water uptake is not limited by the availability of soil moisture ($\theta > \theta_c$). Since high S will ultimately lead to low θ, $\overline{\theta' S'} < 0$.

[16] For the VCR-LTER data, this behavior is almost opposite (Figure 3b). The (small) initial increase in σ_s during July (Figures 2 and 3), is due to heterogeneous but unstressed transpiration ($\overline{\theta' S'} < 0$). However, the coarse grained soils in combination with high E_p lead to rapid soil moisture limitation on S. This causes a sharp decrease in variance ($\overline{\theta' S'} > 0$) during August. Similar to the Louvain-la-Neuve case, rainfall events in September force σ_s to readjust to the soil footprint, causing $\overline{\theta' q'} < 0$. Here a spatially variable q causes an increase rather than a decrease in spatial variance of θ.

[17] Tarrawarra shows a more complex pattern (Figure 3c). In southern hemisphere spring (September–November), vegetation controls act to create variance ($\overline{\theta' S'} < 0$). This variance is initially destroyed by drainage of rainfall. In this period, drying of the soil ($d\overline{\theta}^2/dt < 0$) causes a transition from non-local to local controls on σ_s [Grayson et al., 1997]. This can be seen by the negative landscape contributions. Later during summer (December–February), soil and landscape controls become effectively zero due to advanced drying. The strong soil controlled root water uptake ($\theta < \theta_c$) causes a transition of the sign of the correlation between S and θ ($\overline{\theta' S'} > 0$) resulting in a strong decrease in σ_s^2. The readjustment to the winter soil moisture state is accompanied by an increase in σ_s^2 caused by both soil and (non-local) landscape controls.

5. Discussion

[18] Our simulations show that both soil and vegetation controls can act to either create or destroy spatial variance. The main discriminating factor between both behaviors is whether or not the soil dries below θ_c. This depends on the soil texture as well as on the maximum precipitation deficit, which can show considerable interannual variability in many regions. Including the effects of interannual variability in meteorological forcing on soil moisture variability might be subject of future research. The fact that much of the observed soil moisture variability is actually created by vegetation anomalies (and thus $\rho(\theta, \xi) \neq 0$) calls for new approaches to the soil moisture aggregation problem. This suggests that future field campaigns can further contribute to our understanding of the soil-vegetation-atmosphere

system not only by looking at soil moisture variability, but also at how this variability is related to anomalies in soil and vegetation characteristics.

References

Albertson, J., and G. Kiely (2001), On the structure of soil moisture time series in the context of land surface models, *J. Hydrol.*, *243*, 101–119.

Albertson, J., and N. Montaldo (2003), Temporal dynamics of soil moisture variability: 1. Theoretical basis, *Water Resour. Res.*, *39*(10), 1274, doi:10.1029/2002WR001616.

Al-Kaisi, M., L. Brun, and J. Enz (1989), Transpiration and evapotranspiration from maize as related to leaf area index, *Agric. For. Meteorol.*, *48*, 111–116.

Campbell, G. (1974), A simple method for determining unsaturated conductivity from moisture retention data, *Soil Sci.*, *117*(6), 311–314.

Charpentier, M., and P. Groffman (1992), Soil moisture variability within remote sensing pixels, *J. Geophys. Res.*, *97*(D17), 18,987–18,995.

Clapp, R., and G. Hornberger (1978), Empirical equations for some soil hydraulic properties, *Water Resour. Res.*, *14*(4), 601–604.

Crow, W., and E. Wood (2002), Impact of soil moisture aggregation on surface energy flux prediction during SGP'97, *Geophys. Res. Lett.*, *29*(1), 1008, doi:10.1029/2001GL013796.

Famiglietti, J., J. Rudnicki, and M. Rodell (1998), Variability in surface moisture content along a hillslope transect: Rattlesnake Hill, Texas, *J. Hydrol.*, *210*, 259–281.

Famiglietti, J., J. Devereaux, C. Laymon, T. Tsegaye, P. Houser, T. Jackson, S. Graham, M. Rodell, and P. Oevelen (1999), Ground-based investigation of soil moisture variability within remote sensing footprints during the Southern Great Plains 1997 (SGP97) Hydrology Experiment, *Water Resour. Res.*, *35*(6), 1839–1851.

Grayson, R., A. Western, F. Chiew, and G. Blöschl (1997), Preferred states in spatial soil moisture patterns: Local and nonlocal controls, *Water Resour. Res.*, *33*(12), 2897–2908.

Hawley, M., T. Jackson, and R. McCuen (1983), Surface soil moisture variation on small agricultural watersheds, *J. Hydrol.*, *62*, 179–200.

Hupet, F., and M. Vanclooster (2002), Intraseasonal dynamics of soil moisture variability within a small agricultural maize cropped field, *J. Hydrol.*, *261*, 86–101.

Hupet, F., and M. Vanclooster (2004), Sampling strategies to estimate field areal evapotranspiration fluxes with a soil water balance approach, *J. Hydrol.*, *292*, 262–280, doi:10.1016/j.jhydrol.2004.01.006.

Koster, R., M. Suarez, R. Higgins, and H. van den Dool (2003), Observational evidence that soil moisture variations affect precipitation, *Geophys. Res. Lett.*, *30*(5), 1241, doi:10.1029/2002GL016571.

Laio, F., A. Porporato, L. Ridolfi, and I. Rodriguez-Iturbe (2001), Plants in water-controlled ecosystems: Active role in hydrologic processes and response to water stress: II. Probabilistic soil moisture dynamics, *Adv. Water Resour.*, *24*, 707–723.

Owe, M., E. Jones, and T. Schmugge (1982), Soil moisture variation patterns observed in Hand County, South Dakota, *Water Resour. Bull.*, *18*(6), 949–954.

Salvucci, G. (1998), Limiting relations between soil moisture and soil texture with implications for measured, modeled and remotely sensed estimates, *Geophys. Res. Lett.*, *25*(10), 1757–1760.

Svetlitchnyi, A., S. Plotnitskiy, and O. Stepovaya (2003), Spatial distribution of soil moisture content within catchments and its modelling on the basis of topographic data, *J. Hydrol.*, *277*, 50–60.

Western, A., and R. Grayson (1998), The Tarrawarra data set: Soil moisture patterns, soil characteristics, and hydrological flux measurements, *Water Resour. Res.*, *34*(10), 2765–2768.

Western, A., S. Zhou, R. Grayson, T. McMahon, G. Blöschl, and D. Wilson (2004), Spatial correlation of soil moisture in small catchments and its relationship to dominant spatial hydrological processes, *J. Hydrol.*, *286*, 113–134.

————————————

A. J. Teuling and P. A. Troch, Hydrology and Quantitative Water Management Group, Wageningen University, Nieuwe Kanaal 11, NL-6709 PA, Wageningen, Netherlands. (ryan.teuling@wur.nl)